Prediction of the microstructure morphology after the WAAM process based on the FEM simulation results

SZYNDLER Joanna[1,a*], APEL Markus[2,b] and HÄRTEL Sebastian[1,c]

[1]Chair of Hybrid Manufacturing, Brandenburg University of Technology, Cottbus, Germany

[2]ACCESS e.V., Aachen, Germany

[a] Joanna.Szyndler@b-tu.de, [b]M.Apel@access-technology.de, [c]Sebastian.Haertel@b-tu.de

Keywords: Finite Element Method (FEM), Wire Arc Additive Manufacturing (WAAM), Microstructure Prediction, Phase Field Method

Abstract. To improve understanding of the material behavior of additive-produced components, this paper focuses on the development of a numerical model that reproduces a Wire Arc Additive Manufacturing (WAAM) process, with particular attention given to the evolution of the microstructure. In this study, a finite element model in Simufact Welding software is developed, that replicates a real wire arc welding process of building a multilayer straight wall. Microscopy analysis of the weld wall cut in the middle of its length gave information about the expected microstructure morphology at different levels of the build wall. The whole experimental setup is reproduced in the software Simufact Welding. Simulation results in the form of temperature-time and temperature gradient-time history are then used as superimposed thermal conditions to simulate the microstructure evolution at different areas of the welded part by using MICRESS software.

Introduction

Because of the many advantages of the WAAM process, this welding technique is becoming more and more popular in many engineering industries [1-5], hence it is also in focus of many research works in many research centers all over the world [6-11]. There is almost no limitation in the desired shapes of manufactured parts and a wide range of different materials is applicable. WAAM can be combined with other manufacturing processes to improve the functionality of the desired parts by e.g. adding additional features or it can be used to repair already damaged parts. What is more, with the WAAM process better mechanical properties of the final part can be obtained in comparison to the conventional manufacturing processes such as forging or casting. However, the main advantage of WAAM over other Additive Manufacturing (AM) processes is a shorter time of production and a larger achievable size of the final part [12, 13].

The WAAM process enables the creation of the desired geometry of the final part by depositing subsequent layers of the molten metal on top of each other. By this, a series of heating and cooling cycles take place during this process, which strongly influences a chemical-metallurgical reaction in liquid metal, phase transformations, grain nucleation, its growth, and finally material mechanical properties of the obtained part [14]. Nowadays, different numerical tools are available to simulate the material behavior in different process conditions while minimizing the amount of necessary expensive experimental investigations. To complement experiments, not only Finite Element Models (FEM) [15, 16 - 20] but also neural networks [19, 21, 22], mathematical [23] or recursive models [24] are nowadays increasingly used.

In this work, advantages of the application of a finite element model coupled with a phase-field simulation are discussed which delivers results about the material microstructure evolution during the WAAM process, i.e. can elucidate the process-microstructure relation for a WAAM process. The simulation results are confronted with experimental data to validate the simulations.

Experimental procedure

The welding experiments have been conducted with an Arc 605 WAAM system of GEFERTEC GmbH (Berlin, Germany) at room temperature. Nine 300 mm long seams of SG2 wire (Ø1.2 mm) are welded one on top of the other on a C45 plate giving a 15 mm height wall. A time break between welding each layer was set to 38 s and the welding direction was reversed after each layer. The precise description of the developed setup is presented in earlier Authors' work [25].

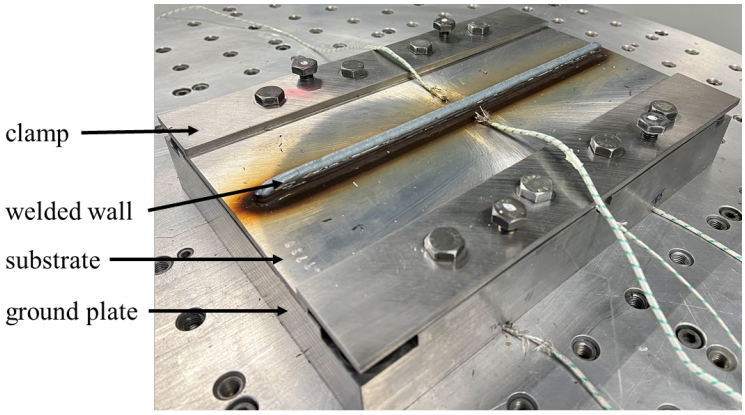

Fig. 1. Experimental setup for welding experiment.

Then, a microscopy analysis using SEM was made at the cross-section at two selected locations in the middle of the welded wall (V1) as presented in Fig 2a and b. Obtained results (Fig. 2c) reveal a mostly ferritic microstructure in the areas pointed as P1 and P2 in Fig. 2b, which were chosen for further analysis. To measure the average grain size an intercept technique was applied [26]. The measured average grain size at the level of the third welded layer (area P1) equals ca 8.08 µm. In location P2 in the middle of the last welded layer, the observed microstructure is more irregular than in location P1. The visible structure contains very big and very small grains, where the measured average grain size is approximately 3.67 µm.

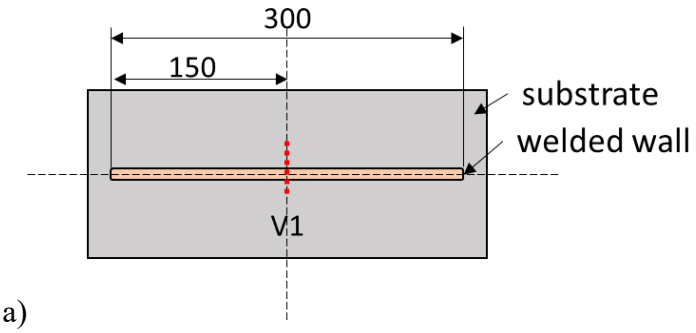

a)

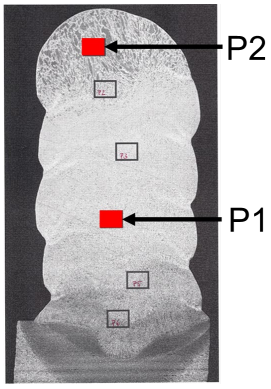

b)

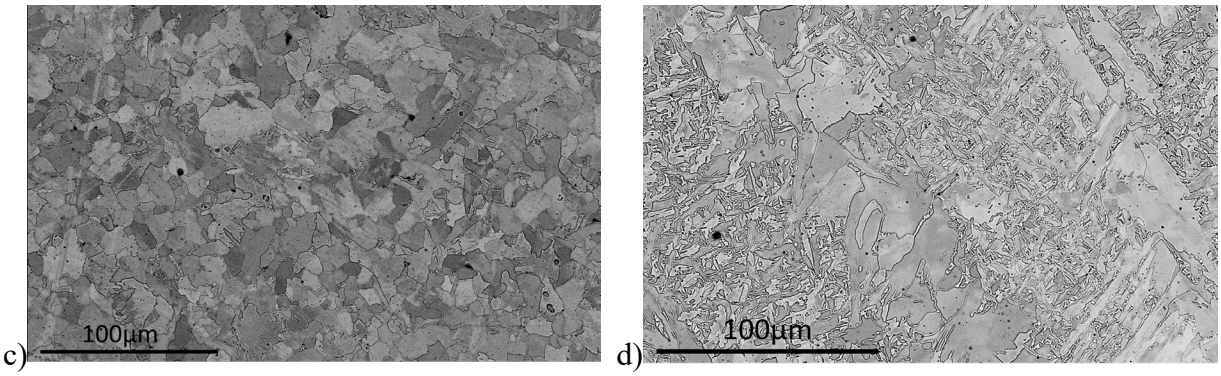

Fig. 2. a) Locations of the microstructure analyses; b) cross-section of the welded wall; zoom at the microstructure morphology at the location c) P1 and d) P2.

The next step was to reproduce experimentally obtained results by the development of the numerical model on the macro- and micro-scale.

Numerical simulation – macro-scale model

A numerical model that reproduces the experimental setup in a digital form is developed in the Simufact.Welding 2021.1 software (Hexagon, Stockholm). The whole setup including a ground plate, substrate plate, and holding clamps was modeled (Fig 3a). A difference in the obtained thickness of each welded layer observed during the experiment was also considered in the numerical simulation model (Fig 3b).

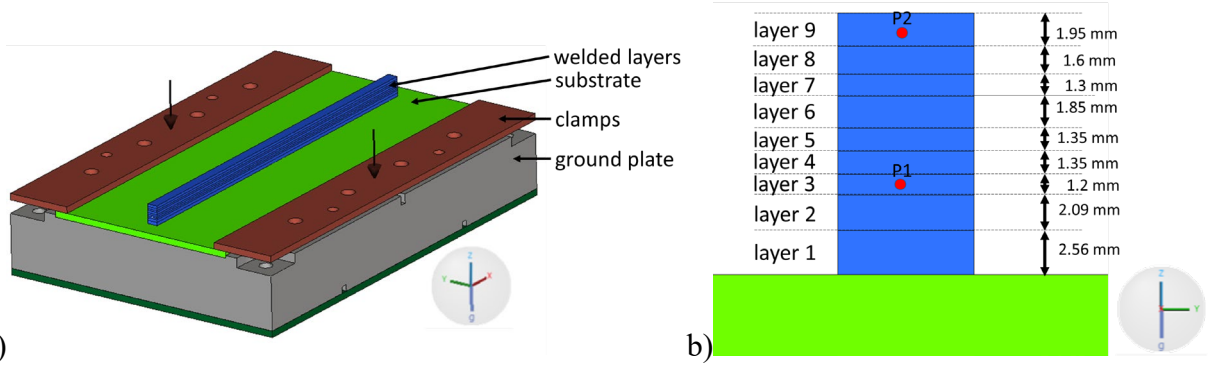

Fig. 3. FE model developed in Simufact. Welding software: a) full setup, b) cross-section of the weld seam.

Thermal parameters, such as the density and thermal capacity of the AISI 1045 steel substrate, were taken from the literature [27, 28] (Fig. 4a, b). The values of the thermal conductivity were measured by the Authors with Linseis LFA 1000 Laser Flash test machine (**Linseis Messgeräte GmbH, Selb, Germany)** (Fig. 4c), whereas the applied convective heat transfer parameters were determined in earlier Authors' work [25]. Material properties of the SG2 wire are taken from the Simufact.Welding 2021.1 material database.

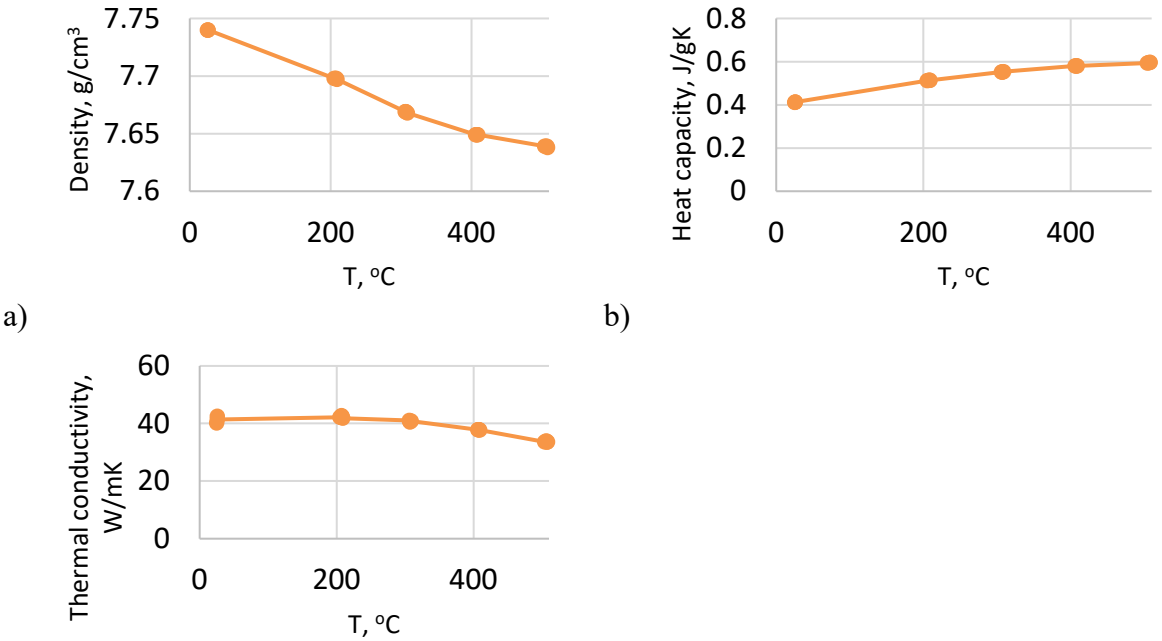

Fig. 4. Material properties of AISI 1045 as a function of temperature: a) density [27], b) heat capacity [28], c) thermal conductivity measured by Authors.

Simulation of welding a nine-layer wall was performed with the same speed (400 mm/min), voltage (14.6 V), and current (144 A) as welding parameters applied during the real experiment. Also, the 38 s-time break between welded layers as well as reversing the welding direction after each layer was also applied. The air temperature and initial temperature of the wire were set to 23°C, the initial temperature of all plates was set to 21.5°C, and arc efficiency was assumed to be 80%. The Goldaks' heat source model [29] was used to describe the volumetric heat flux density distribution, where a_f, a_r, b, d are parameters related to the shape characteristic of the welding arc. A two-heat source model was applied with parameters whose exact values and optimization procedure are described in earlier Authors' work [25]. An example of the predicted temperature history and temperature gradient at selected points (see Fig. 3b) is presented in Fig. 5. The temperature history and also temperature gradients are later necessary for the MICRESS simulation.

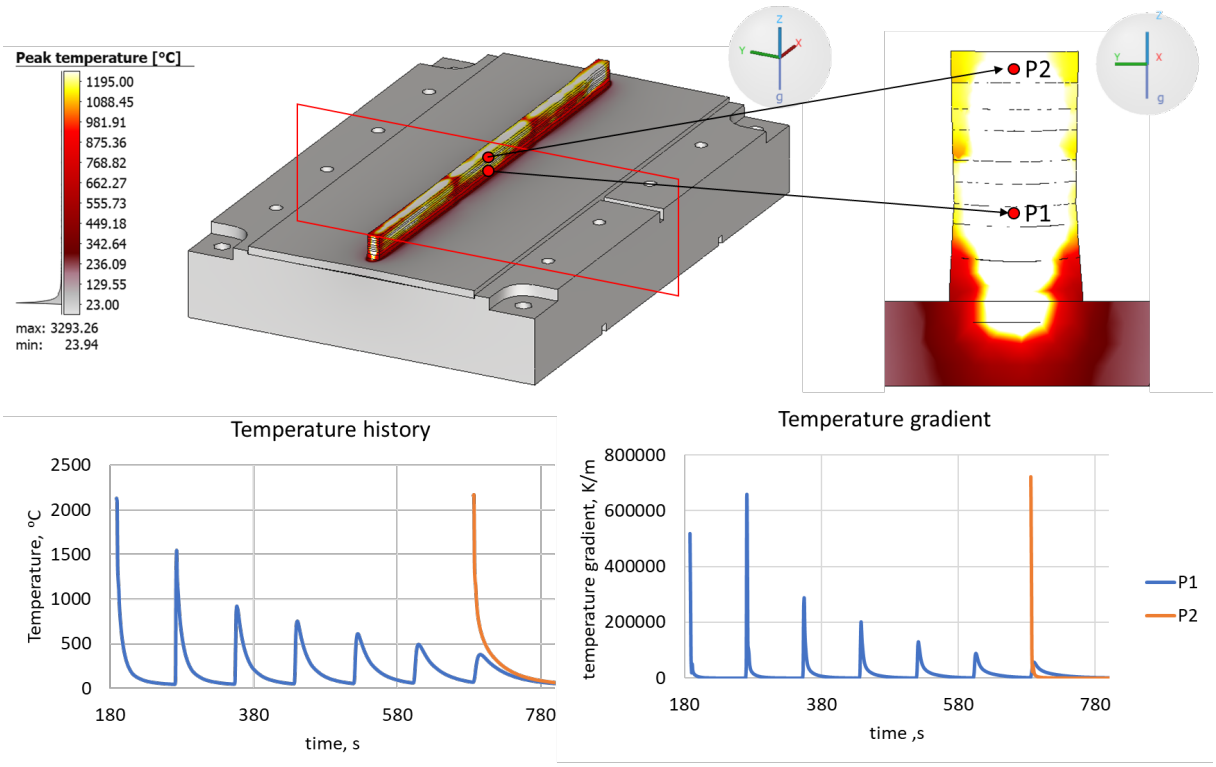

Fig. 5. Simulation results in the form of peak temperature distribution at the cross-section with the visualization of the temperature-time and temperature gradient-time plots obtained at points P1 and P2.

Microscale simulation

To simulate the material response and its microstructure evolution, two software packages were used: the thermodynamic software ThermoCalc [30] and the phase-field software MICRESS [31]. With ThermoCalc, a GES5 file was generated from the database TCFE12. The GES5 file is a subset of the thermodynamic database with selected alloying elements and phases and is used as a basis for the thermodynamic material model, in particular for the driving force calculations in MICRESS. According to the chemical composition of the wire, the GES5 file contains the elements Fe, C, Mn, Ni, and Si and the three phases Liquid, FCC, and BCC. The initial chemical composition of the melt and thus the material description for the simulation is given in Tab. 1. Details about the underlying phase-field model, the coupling between thermodynamic and phase-field calculations, and further examples for modeling phase transformations in steel with MICRESS can be found e.g. in [32-35].

Table 1. The initial concentration of components in the liquid phase

C%	Mn%	Ni%	Si%
0.1	1.1	0.15	0.65

Time-temperature and time-temperature-gradient plots (Fig. 5) were extracted from the FE macro-scale simulation at the selected locations P1 and P2 and imported as superimposed thermal conditions by the microscale model in the MICRESS software. Whereas the phase-field model is a quantitative and predictive model for phase transformations, i.e. growing interfaces, the phenomenological nucleation model in MICRESS requires a parameter calibration to obtain a quantitative fit between simulation and real data. This was done by a manual optimization procedure, where the nucleation barrier and the minimum distance of nucleating grains were

adjusted. Simulated microstructure morphologies, time–phase fraction plots, and the average grain size were used for the validation with the experimental measurements. The average size at location P1 at the end of the simulation equals 6.6 μm and 4.7 μm at location P2. The grain morphology in the last welded layer predicts the elongated shape of all grains with a big disproportion in their sizes (Fig. 6a). As expected, at the first stage of the cooling of the 9th layer, a quick solidification process is observed where a fully ferritic (δ) structure is obtained (Fig. 6b). Then, as the temperature drop continues, almost half of the examined area transforms into austenite and most of it back again into ferrite (α). At the end of the simulation, an almost fully ferritic structure is observed. Figures 6 c-e present an example of obtained results during the very first stage of the cooling process at 1.45s, which are additional information provided by the phase field model, that could be also used for a subsequent analysis of material properties. In Fig. 6c where a phase fraction concentration is presented, red color refers to the liquid phase and yellow to the ferrite phase. Distributions of the carbon and manganese concentrations are presented in Figs 6d and 6e respectively.

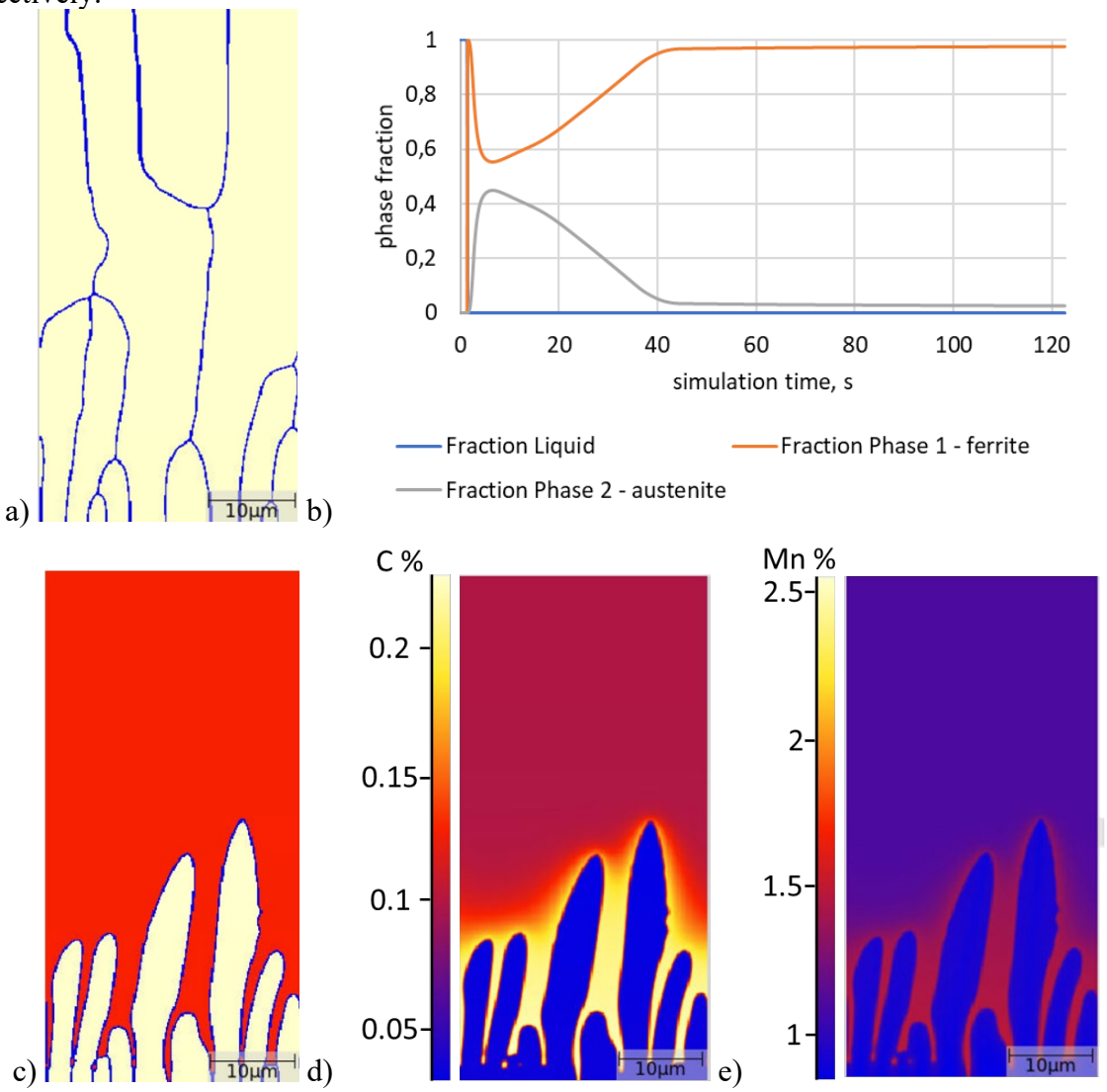

Fig. 6. a) Ferritic grain structure at the end of the process and b) simulated phase fraction evolution at P2; c) Ferritic solidification morphology, d) Carbon, and e) Manganese concentration distributions during solidification, snapshots at 1.45 s.

When the results obtained in the middle of the 3rd welded layer are analyzed, much different grain shapes are predicted than in the 9th layer. Still, some smaller grains with elongated shapes

are visible, but the bigger ones have more uniform shapes (Fig. 7a). This is caused by a reheating cycle (see Fig. 5) when further layers were applied, which caused grain growth and nucleation of new ones. Figure 7b presents the influence of the multiple reheating of the material on the phase fraction history.

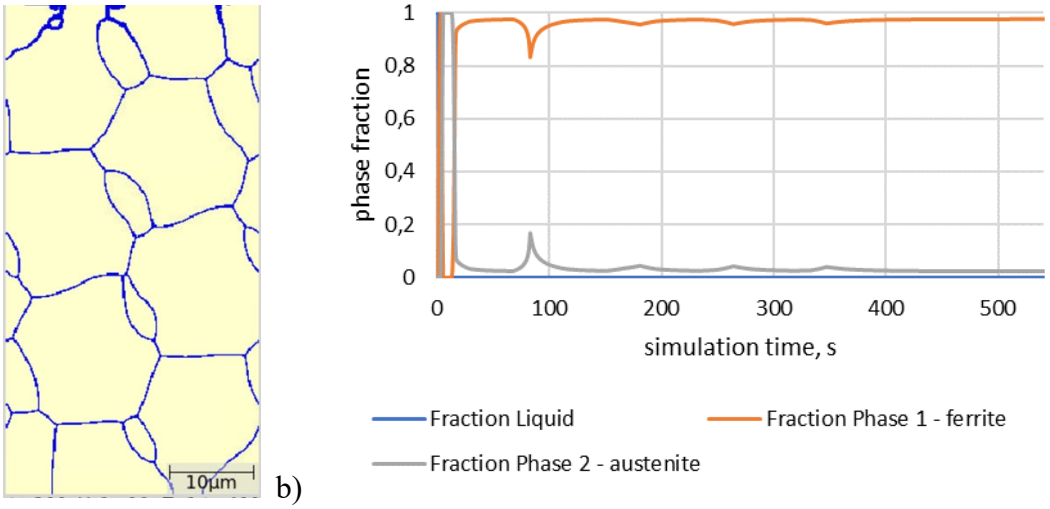

Fig 7. a) Microstructure morphology and b) phase fraction evolution at P1 obtained due to the simulation.

Validation of the numerical simulation results

For the validation stage, a smaller area of the SEM picture was selected, that correlates with the size of the microstructure calculated in the MICRESS software. In both locations, a good match between the shapes of obtained grains is visible (Fig. 8) as well as the average grain size is well predicted, which is equal to 5.7 µm (4.7 µm in simulation) in location P1 and 6.5 µm (6.5 µm in simulation) in location P2.

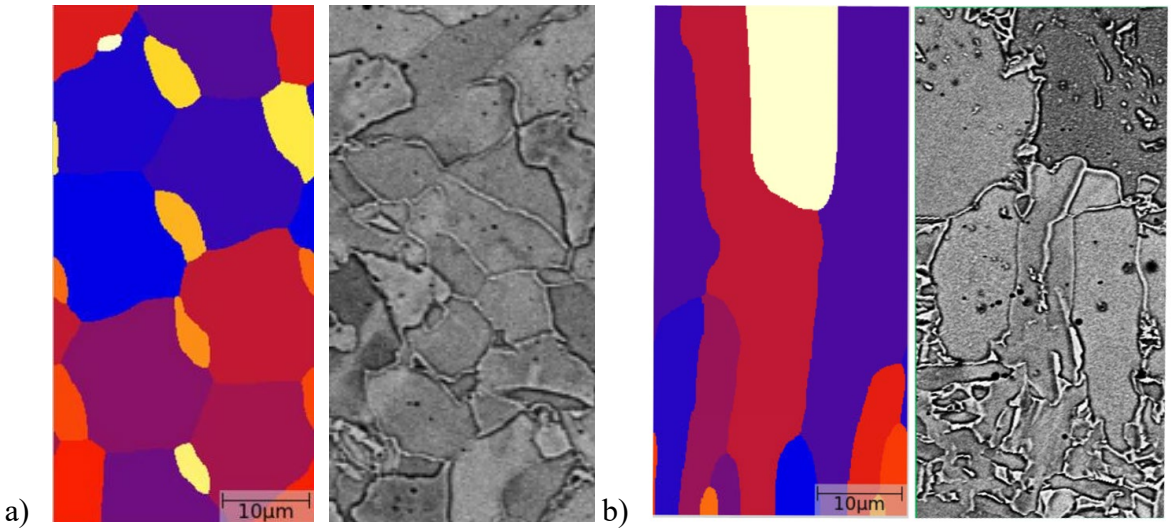

Fig. 8. Comparison between the simulation and real microstructure taken from locations a) P1, b) P2. Different colors refer to the different grains.

The obtained results prove that it is possible to obtain good results from the simulation of the WAAM process, not only at the macro-scale but also at the micro-scale level. Such virtual information about possible material morphology may be a clue for a further determination of other material parameters of the final product, which are influenced by the grain structure.

Conclusions

Within this work, the Authors developed a multiscale solution by combining a macro and micro scale model to predict material microstructures for the WAAM process. Simulation results were validated with experimental results: the grain shapes, as well as the average grain size, were successfully predicted at two different locations of a welded straight wall and the differences are explained by the different thermal histories. One point was selected in the middle of the last welded layer, subjected to only one cycle of heating and cooling. When more layers are applied, lower layers undergo multiple cycles of reheating and cooling which influences the microstructure by ferrite to austenite transformations in combination with grain growth and nucleation.

The results show that the multiscale simulation approach as discussed in the paper can provide a good qualitative prediction of the microstructure evolution in ferritic steel during the WAAM process. This validated model can lead to the provision of a better understanding of the material response and eventually its final properties. A well-developed model can be later used to analyze the influence of the different parameters of the welding on the microstructure in the final part. Microstructural information can be later on used as input for calculating material properties like tensile strength or cyclic fatigue.

Acknowledgments

The Authors acknowledge the Center for Hybrid Electric Systems Cottbus (CHESCO) for their support. This project is funded by the Federal Government in the context of the “Investitionsgesetz Kohleregionen” and co-financed by the State of Brandenburg.

References

[1] V. Madhavadas, D. Srivastava, U. Chadha, S.A. Raj, M.T.H. Sultan, F.S. Shahar, A.U.M. Shah, A review on metal additive manufacturing for intricately shaped aerospace components, CIRP Journal of Manufacturing Science and Technology, 39 (2022) 18-36. https://doi.org/10.1016/j.cirpj.2022.07.005

[2] J. Ye, P. Kyvelou, F. Gilardi, H. Lu, M. Gilbert, L. Gardner, An end-to-end framework for the additive manufacture of optimized tubular structures, IEEE Access, 9 (2021) 165476-165489. https://doi.org/10.1109/ACCESS.2021.3132797

[3] X. Zuo, W. Zhang, Y. Chen, J.P. Oliveira, Z. Zeng, Y. Li, Z. Luo, S. Ao, Wire-based directed energy deposition of NiTiTa shape memory alloys: Microstructure, phase transformation, electrochemistry, X-ray visibility and mechanical properties, Additive Manufacturing, 59 (2022) 103115. https://doi.org/10.1016/j.addma.2022.103115

[4] M. Vishnukumar, R. Pramod, A.R. Kannan, Wire arc additive manufacturing for repairing aluminium structures in marine applications, Materials Letters, 299 (2021) 130112. https://doi.org/10.1016/j.matlet.2021.130112

[5] T. Feucht, J. Lange, B. Waldschmitt, A.K. Schudlich, M. Klein, M. Oechsner, Welding process for the additive manufacturing of cantilevered components with the WAAM, Advanced Joining Processes, 125 (2020) 67-78. https://doi.org/10.1007/978-981-15-2957-3_5

[6] S. Zhou, J. Zhang, G. Yang, Y. Wang, B. Li, D. An, J. Zheng, W. Wei, Microstructure evolution and fracture behavior of Ti–6Al–4V fabricated by WAAM-LDM additive manufacturing, Journal of Materials Research and Technology, 28 (2024) 347-362. https://doi.org/10.1016/j.jmrt.2023.11.255

[7] C. Sasikumar, R. Oyyaravelu, Mechanical properties and microstructure of SS 316 L created by WAAM based on GMAW, Materials Today Communications, 38 (2024) 107807. https://doi.org/10.1016/j.mtcomm.2023.107807

[8] V. Laghi, N. Babovic, E. Benvenuti, H. Kloft, Blended structural optimization of steel joints for Wire-and-Arc Additive Manufacturing, Engineering Structures, 300 (2024) 117141. https://doi.org/10.1016/j.engstruct.2023.117141

[9] P. Kyvelou, C. Huang, J. Li, L. Gardner, Residual stresses in steel I-sections strengthened by wire arc additive manufacturing, Structures, 60 (2024) 105828. https://doi.org/10.1016/j.istruc.2023.105828

[10] A.Staroselsky, D. Voytovych, R. Acharya, Prediction of Ni-based alloy microstructure in wire arc additive manufacturing from cellular automata model, Computational Materials Science, 233 (2024) 112721. https://doi.org/10.1016/j.commatsci.2023.112721

[11] H. Mu, F. He, L. Yuan, H. Hatamian, P. Commins, Z. Pan, Online Distortion Simulation Using Generative Machine Learning Models: A Step Toward Digital Twin of Metallic Additive Manufacturing, Journal of Industrial Information Integration, (2024) 100563. https://doi.org/10.1016/j.jii.2024.100563

[12] S.I. Evans, J. Wang, J. Qin, Y. He, P. Shepherd, J. Ding, A review of WAAM for steel construction – Manufacturing, material and geometric properties, design, and future directions, Structures, 44 (2022) 1506-1522. https://doi.org/10.1016/j.istruc.2022.08.084

[13] S. Singh, S.K. Sharma, D.W. Rathod, A review on process planning strategies and challenges of WAAM, Materials Today: Proceedings, 47, 19 (2021) 6564-6575. https://doi.org/10.1016/j.matpr.2021.02.632

[14] A.S. Azar, S.K. As, O.M. Akselsen, Determination of welding heat source parameters from actual bead shape, Computational Material Science, 54 (2012) 176-182. https://doi.org/10.1016/j.commatsci.2011.10.025

[15] X. Zhou, H. Zhang, G. Wang, X. Bai, Three-dimensional numerical simulation of arc and metal transport in arc welding based additive manufacturing, International Journal of Heat and Mass Transfer, 103 (2016) 521-537. https://doi.org/10.1016/j.ijheatmasstransfer.2016.06.084

[16] Z. Hu, X. Qin, T. Shao, Welding thermal simulation and metallurgical characteristics analysis in WAAM for 5CrNiMo hot forging die remanufacturing, Procedia Engineering, 207 (2017) 2203-2208. https://doi.org/10.1016/j.proeng.2017.10.982

[17] C.T.J. Panicker, K.R. Surya, V. Senthilkumar, Novel process parameter-based approach for reducing residual stresses in WAAM, Materials Today: Proceedings, 59 (2022) 1119-1126. https://doi.org/10.1016/j.matpr.2022.03.025

[18] N.P. Gokhale, P. Kala, Thermal analysis of TIG-WAAM based metal deposition process using finite element method, Materials Today: Proceedings, 44 (2021) 453-459. https://doi.org/10.1016/j.matpr.2020.09.756

[19] Y. Ling, J. Ni, J. Antonissen, H.B. Hamouda, J.V. Voorde, M.A. Wahab, Numerical prediction of microstructure and hardness for low carbon steel wire Arc additive manufacturing components, Simulation Modelling Practice and Theory, 122 (2023) 102664. https://doi.org/10.1016/j.simpat.2022.102664

[20] V. Gornyakov, Y. Sun, J. Ding, S. Williams, Modelling and optimizing hybrid process of wire arc additive manufacturing and high-pressure rolling, 223 (2022) 111121. https://doi.org/10.1016/j.matdes.2022.111121

[21] S. Bose, A. Biswas, Y. Tiwari, M. Mukherjee, S.S. Roy, Artificial neural Network-based approaches for Bi-directional modelling of robotic wire arc additive manufacturing, Materials Today: Proceedings, 62, 12 (2022) 6507-6513. https://doi.org/10.1016/j.matpr.2022.04.331

[22] Y. Wang, X. Xu, Z. Zhao, W. Deng, J. Han, L. Bai, X. Liang, J. Yao, Coordinated monitoring and control method of deposited layer width and reinforcement in WAAM process, Journal of Manufacturing Process, 71 (2021) 306-316. https://doi.org/10.1016/j.jmapro.2021.09.033

[23] W.C. Ke, J.P. Oliveira, B.Q. Cong, S.S. Ao, Z.W. Qi, B. Peng, Z. Zeng, Multi-layer deposition mechanism in ultra high-frequency pulsed wire arc additive manufacturing (WAAM) of NiTi shape memory alloys, Additive Manufacturing, 50 (2022) 102513. https://doi.org/10.1016/j.addma.2021.102513

[24] C. Chen, H. He, J. Zhou, G. Lian, X. Huang, M. Feng, A profile transformation based recursive multi-bead overlapping model for robotic wire and arc additive manufacturing (WAAM), Journal of Manufacturing Processes, 84 (2022) 886-901. https://doi.org/10.1016/j.jmapro.2022.10.042

[25] J. Szyndler, A. Schmidt, S. Härtel, Determination of welding heat source parameters for FEM simulation based on temperature history and real bead shape. Materials Research Proceedings 28 (2023) 159-168. https://doi.org/10.21741/9781644902479-18

[26] ISO 643:2019 - Steels — Micrographic determination of the apparent grain size

[27] M. Hojny, M. Glowacki, Numerical Modelling of Steel Deformation at Extra-High Temperatures, in P. Miidla (ed.), Numerical Modelling, IntechOpen, London, 2012, 10.5772/36562. https://doi.org/10.5772/36562

[28] A. Martinovs, S. Polukoshko, E. Zaicevs, R. Revalds, Laser Hardening Process Optimizations Using FEM, Engineering for Rural Development, 2020. https://doi.org/10.22616/ERDev.2020.19.TF372

[29] J. Goldak, A.P. Chakravarti, M. Bibby, A new finite element model for welding heat sources, Metallurgical Transactions B, 15 (1984) 299-305. https://doi.org/10.1007/BF02667333

[30] Computational Materials Engineering - Thermo-Calc Software (thermocalc.com)

[31] MICRESS 7.1: http://www.micress.de.

[32] B. Böttger, M. Apel, M. Budnitzki, J. Eiken, G. Laschet, B. Zhou, Calphad coupled phase-field model with mechano-chemical contributions and its application to rafting of γ' in CMSX-4. Computational Materials Science, 184 (2020) 109909. https://doi.org/10.1016/j.commatsci.2020.109909

[33] B. Böttger, J. Eiken, M. Apel, Multi-ternary extrapolation scheme for efficient coupling of thermodynamic data to a multi-phase-field model, Computational Materials Science, 108 (2015) 283–292. https://doi.org/10.1016/j.commatsci.2015.03.003

[34] B. Böttger, M. Apel, T. Jokisch, A. Senger, Phase-field study on microstructure formation in Mar-M247 during electron beam welding and correlation to hot cracking susceptibility. IOP Conference Series: Materials Science and Engineering, 861 (2020) 012072. https://doi.org/10.1088/1757-899X/861/1/012072

[35] B. Böttger, M. Apel, J. Eiken, P. Schaffnit, I. Steinbach, "Phase-Field Simulation of Solidification and Solid-State Transformations in Multicomponent Steels", Steel Research International. 79 (2008) 608. https://doi.org/10.1002/srin.200806173